Molecular BioSystems

PAPER

View Article Online
View Journal | View Issue

Cite this: *Mol. BioSyst.*, 2016, 12, 2541

Discovery of a potent cyclooxygenase-2 inhibitor, S4, through docking-based pharmacophore screening, *in vivo* and *in vitro* estimations

Tien-Sheng Tseng,†[ab] Show-Mei Chuang,†[c] Nai-Wan Hsiao,[d] Yi-Wen Chen,[e] Yu-Ching Lee,[fg] Chi-Chen Lin,[c] Cheng Huang[a] and Keng-Chang Tsai*[ag]

Received 29th March 2016,
Accepted 26th May 2016

DOI: 10.1039/c6mb00229c

www.rsc.org/molecularbiosystems

Cyclooxygenase (COX; EC: 1.14.99.1), the key enzyme in prostaglandin production in the human body, is a major pharmacological target for developing anti-inflammatory agents. Nonsteroidal anti-inflammatory drugs exhibit anti-inflammatory and analgesic activities when inhibiting COX-2 but cause gastrointestinal toxicity and other side effects because of concurrent inhibition of COX-1. Thus, potent and safe inhibitors against COX-2 are urgently required. We constructed a novel docking-based pharmacophore model for screening selective COX-2 inhibitors and discovered compounds **S1**, **S2**, **S3**, and **S4**, which apparently inhibit COX-2. Particularly, **S4** inhibits COX-2 *in vitro* and shows a potent anti-inflammatory effect *in vivo* without cytotoxicity. Molecular docking analyses revealed that **S4** interacted satisfactorily with the active site of COX-2 but not with that of COX-1. This reveals that **S4** more specifically inhibits COX-2 and has potential for application in developing anti-inflammatory and anticancer agents.

1. Introduction

Cyclooxygenase (COX; EC 1.14.99.1), the prostaglandin G/H synthase or endoperoxide synthase, is a crucial enzyme for converting arachidonic acid to prostaglandins. COX exists in two main isoforms, COX-1 and COX-2. COX-1 is expressed constitutively in almost all mammalian cells and involved in homeostasis,[1–3] whereas COX-2 is inducibly expressed and involved in inflammatory processes.[4–6] COX-2 overexpression is associated with some human cancers, such as colon, gastric, breast, and lung cancers and hepatocellular carcinoma.[7,8] In addition, COX-2 is expressed at high levels in tumors and inflammatory lesions but not in normal cells. Moreover, activated COX-2 can stimulate several major steps in tumor development, including metastasis, angiogenesis, cell division, and cell death inhibition.[11,12] Colorectal cancer could be driven by chronic inflammation, in which COX-2 is the most critical gene involved in tumor metastasis.[13] Thus, COX-2 is an attractive target to develop anti-inflammatory, antitumor, and antimetastatic therapeutic agents.

Nonsteroidal anti-inflammatory drugs (NSAIDs) are therapeutic agents extensively used in treating inflammatory diseases, including osteoarthritis (OA) and rheumatoid arthritis (RA), by suppressing COX activity.[14] The analgesic and anti-inflammatory activities of NSAIDs are based on COX-2 inhibition, but simultaneous COX-1 inhibition causes gastrointestinal (GI) toxicity and other side effects, such as GI tract bleeding, perforation, and ulcers.[15–17] Therefore, inhibitors selectively abolishing COX-2 activity but sparing COX-1 activity are urgently needed for developing safer NSAIDs.[18–22] COX-2-selective inhibitors were initially used as anti-inflammatory agents; their GI side effects were lower than those of NSAIDs. These COX-2 inhibitors exhibited antiangiogenic activity *in vitro* and inhibited tumor growth in animal studies.[23] The ability of COX-2-selective inhibitors to decrease the hematogenous metastasis of COX-2-expressing tumors and their antiangiogenic effects increase the probability of their high efficacy in preventing and treating some cancers.[24] In addition, some COX-2 inhibitors have been studied in the treatment of neurodegenerative diseases, such as Alzheimer disease.[25,26] The first-generation COX-2-selective NSAIDs are rofecoxib and celecoxib.[27] Rofecoxib selectively inhibits COX-2 and has little affinity for COX-1. Unlike non-selective NSAIDs, rofecoxib does not inhibit platelet aggregation.[28] Celecoxib, a selective noncompetitive inhibitor of COX-2, binds with its polar sulfonamide side chain to a hydrophilic side pocket

[a] *National Research Institute of Chinese Medicine, Ministry of Health and Welfare, Taipei, Taiwan. E-mail: tkc@nricm.edu.tw; Fax: +886-2-7211156; Tel: +886-2-28201999 ext 6241*
[b] *Institute of Biomedical Sciences, Academia Sinica, Taipei 115, Taiwan*
[c] *Institute of Biomedical Sciences, National Chung Hsing University, Taichung, Taiwan*
[d] *Institute of Biotechnology, National Changhua University of Education, Changhua, Taiwan*
[e] *Cold Spring Biotech Corp., Taiwan*
[f] *The Center of Translational Medicine, Taipei Medical University, Taipei, Taiwan*
[g] *The Ph.D. Program for Medical Biotechnology, College of Medical Science and Technology, Taipei Medical University, Taipei 110, Taiwan*
† These corresponding authors contributed equally to this work.

region close to the active COX-2 binding site,[4,29–32] The second-generation COX-2-selective NSAIDs are etoricoxib and valdecoxib.[27] Etoricoxib selectively inhibits COX-2 and reduces prostaglandins (PGs) generation from arachidonic acid.[33–35] Valdecoxib, a selective cyclooxygenase-2 (COX-2) inhibitor, is used for its anti-inflammatory, analgesic, and antipyretic activities in the management of osteoarthritis (OA). Different from celecoxib, valdecoxib lacks a sulfonamide chain and does not require CYP450 enzymes for metabolism.[36] However, these selective COX-2 inhibitors, eoticoxib, valdecoxib, and celecoxib cause GI damage[37–40] and other side effects. Celecoxib increases the incidence of major vascular events, including nonfatal myocardial infarction and nonfatal stroke,[41] and the long-term, high-dose use of rofecoxib increases the risk of heart attack and stroke. These adverse cardiovascular side effects of selective COX-2 inhibitors have raised safety concerns.[42] Thus, selective, potent, and safe COX-2 inhibitors that can completely supersede narcotic and steroidal drugs are urgently required.

The protein structures of COX-1 and COX-2 are highly conserved, which contains three functional domains: an epidermal growth factor-like domain (N-terminal), a membrane bound domain (MBD) and a globular catalytic domain (C-terminal). The active site of COX, spreading from the MBD to the interior of the catalytic domain, has the binding capacity of substrates or inhibitors such as nonsteroidal anti-inflammatory drugs (NSAIDs).[43] However, a side pocket of COX active site, at the interface between the MBD and the catalytic domain, composed of three residues (Arg-120, Tyr-355, and Glu-524) that affects the specificity of inhibitors or substrates to COX-1 or COX-2.[44,45] In addition, part of the MBD structure in COX-2 differs from COX-1 which leading to enlarge the solvent-accessible surface area at the interface between the MBD and the active site of COX-2. These characters imply that COX active site could be a select target for inhibitors.[45,46] Computer-aided drug design has been widely used to discover lead compounds in the initial phase of drug development. Structure- and ligand-based drug designs are efficient methods to rationally identify novel inhibitors. Structure-based virtual screening (molecular docking) can recognize potential bioactive compounds from their structural characteristics; this technique is inexpensive and less time intensive. These benefits along with the established structure of COX-2 [Protein Data Bank (PDB) ID: 1CX2] render feasible the screening of potent COX-2 inhibitors through molecular docking. For a more precise identification of potent COX-2 inhibitors, the functional features necessary for complementary interaction with COX-2 active sites must be considered. Ligand-based pharmacophore modeling efficiently and precisely recognizes the functional features of compounds critical for specific compound-receptor interactions. To design and discover potent COX-2 inhibitors, we constructed a docking-based pharmacophore (**DBP**) model.

We used molecular docking and pharmacophore modeling to construct the **DBP** model, in which the best hypothesis, **Hypo1**, was used for screening novel COX-2 inhibitors. Approximately 420 000 compounds from the InterBioScreen synthetic database (IBS Inc.; http://www.ibscreen.com) were reduced to 2258 potential candidates through ligand pharmacophore mapping. Subsequently, docking algorithms GOLD[47,48] and CDOCKER[49–52] were used to confirm and analyze the potential interactions of these compounds with COX-2, following which 61 of the 2,258 compounds were examined for their COX-2 inhibitory ability. COX-2 inhibition assays revealed that compounds **S1** (IBS Catalog ID: STOCK3S-81120), **S2** (STOCK1S-15490), **S3** (STOCK4S-51317), and **S4** (STOCK5S-10619) exhibited apparent inhibitory activities against COX-2 (39.4%, 48%, 50%, and 55%, respectively) at 87 μM. Particularly, **S4** exhibited inhibitory activity against COX-2 *in vitro* in addition to demonstrating strong anti-inflammatory activity *in vivo* without causing major cytotoxicity. Moreover, molecular docking analyses revealed that **S4** fitted well in the active site of COX-2 with stable hydrogen bonds (particularly hydrogen bonding with Arg513) and hydrophobic interactions but exhibited considerable steric clash with Ile513 of COX-1. Diverse interactions with these nonconserved active site residues are necessary for the selective inhibition of COX-2, indicating that **S4** has a strong potential as a specific COX-2 inhibitor. This study demonstrated a successful strategy of using molecular docking and ligand-based pharmacophore modeling in combination to construct a novel **DBP** model to screen selective COX-2 inhibitors. **S4**, identified by the **DBP** model, has strong potential for application in developing anti-inflammatory and anticancer agents.

2. Materials and methods

2.1. Materials

The pharmacophore hypotheses generation, ADMET analysis, and CDOCKER molecular docking were implemented by the Discovery Studio 4 (Accelrys Inc., San Diego, CA, USA). The GOLD (Cambridge Crystallographic Data Center (CCDC), version 5.1) docking program with the GoldScore scoring function was applied for molecular docking analysis as well. The 24 COX-2 inhibitors (Fig. 2) used to establish the docking-based pharmacophore (**DBP**) hypotheses were retrieved from literature.[9] Their inhibitory activities (IC_{50}) span five orders of magnitude (1.7–70 000 nM) are shown in Table 1. For molecular docking analysis, we used the crystal structure of COX-2 in complex with inhibitor, SC-558 (PDB ID: 1CX2, resolution: 3.0 Å).

2.2. Methods

2.2.1. Docking-based pharmacophore (DBP) generation. The training set, consisting of 24 known COX-2 inhibitors (Fig. 2), was employed to construct the docking-based pharmacophore (**DBP**). Inhibitory activities (IC_{50}) against COX-2 of the training set inhibitors, ranging from 1.7–70 000 nM covering 5 orders of magnitude, were listed in Table 1. The GOLD molecular docking program was used to generate the docking conformations of each inhibitor (each compound generated 225 random conformations that were subjected to 500 000 GA operations). After that, the top ranked docking poses were further applied for docking-based pharmacophore (**DBP**) construction. Four features, hydrogen-bond acceptor (HBA), hydrogen-bond donor (HBD), hydrophobic aromatic features (HA), and ring aromatic (RA) were selected to generate the pharmacophore

Table 1 Actual and predicted IC_{50} values (nM) of the training-set inhibitors based on the **DBP Hypo1**

	Pharmacophore **Hypo1**				
Compound no.	Actual IC_{50} (nM)	Estimated IC_{50} (nM)	Error[b]	Actual scale[a]	Estimated scale[a]
1	1.7	6.8	4.0	+++	+++
2	3.7	7.1	1.9	+++	+++
3	6	25	4.1	+++	+++
4	8	7.1	−1.1	+++	+++
5	12	100	8.3	+++	+++
6	20	15	−1.3	+++	+++
7	26	12	−2.2	+++	+++
8	85	200	2.4	+++	++
9	510	100	−5.1	++	+++
10	650	930	1.4	++	++
11	770	4000	5.2	++	+
12	1500	51	−30	+	+++
13	1700	2000	1.2	++	++
14	1900	11 000	5.8	++	+
15	2600	3200	1.2	+	+
16	3100	5700	1.8	+	+
17	7900	4900	−1.6	+	+
18	8000	12 000	1.5	+	+
19	10 000	11 000	1.1	+	+
20	12 000	12 000	1.0	+	+
21	31 000	4200	−7.4	+	+
22	43 000	15 000	−2.9	+	+
23	68 000	11 000	−6.2	+	+
24	70 000	56 000	−1.3	+	+

[a] Activity scale: highly active ($IC_{50} \leq 200$ nM, +++), moderately active (200 nM $< IC_{50} \leq 2000$ nM, ++), and inactive ($IC_{50} > 2000$ nM, +). [b] The difference between estimated and actual activity values is represented as an error (ratio between the estimated and actual activities), and it is assigned a negative symbol if the actual activity is higher than the estimated one. (The 24 COX-2 inhibitors used to establish the docking-based pharmacophore (**DBP**) hypotheses were retrieved from literature.[51])

hypothesis by 3D-QSAR Pharmacophore Generation (HypoGen) module in Discovery Studio 4. In addition, the minimum and maximum counts for each feature were set to 0 and 3, the uncertainty value was set to 2 for each inhibitor, and all other parameters were set as default.

2.2.2. Molecular docking analysis. CDOCKER and GOLD molecular docking analyses were utilized to confirm the interactions and orientations of potential candidates (2258 compounds) with COX-2 active site. Firstly, to set up an accurate molecular docking protocol, the structure of COX-2 in complex with inhibitor, SC-558, (PDB ID: 1CX2) was applied for training. The reason choosing this complex structure is that SC-558 is a typical, selective inhibitor against COX-2. Thus, the information of this complex is helpful and used as a standard to identify potent selective inhibitors against COX-2. The inhibitor, SC-558, was successfully redocked into the COX-2 active site by the CDOCKER and GOLD programs. The RMSD of re-docked SC-558 and original crystal SC-558 structure was ~0.5 Å (Fig. 4). The detail parameter setting were descried as follows. The complex structure of COX-2 (PDB ID: 1CX2) was employed for docking calculation, in which inhibitor, SC-558, was set as centroid to define the binding site sphere (8 Å). The CDOCKER molecular docking was applied to simulate high-temperature molecular dynamics and the CHARMm force field was used to generate random ligand conformations. Moreover, the heating and cooling target temperature parameters of simulated annealing were set as 700 and 300, respectively. The docking calculations performed the equilibration and minimization of molecular dynamics (MD), and 10 conformations of top hits were generated for each inhibitor along with the estimated CDCOCKER interaction energy (CIE). For GOLD molecular docking, a genetic algorithm (GA) was used to calculate the inhibitor docking into the COX-2 active site with flexible state. 10 conformations were randomly generated for each inhibitor based on the active site of COX-2 for interaction calculation. These conformations were further subjected to at least 500 000 GA operations to find out the optimal inhibitor-COX-2 interaction poses. During the calculation, the hydrogen-bonding energy, van der Waals energy and ligand torsion strain were taken into account in the Goldscore function.

2.2.3. Evaluation of COX-2 activity. The evaluation of COX-2 activity was determined by using COX2 Inhibitor Screening Assay Kit (Cayman Chemical, Ann Arbor, MI), which measures the production of PGE2-α. Briefly, each inhibitor was incubated with purified human recombinant COX-2 for 10 min at 37 °C. The reaction was initiated by 5 μl of 100 μM arachidonic acid, incubated at 37 °C for 2 minutes, and then terminated with 50 μl of 1 M HCl and 100 μl of 50% saturated stannous chloride. This reduced the PGH2 produced by COX-2 to the more stable PGE2α, which was then quantified by an enzyme immunoassay (EIA) method. The reaction samples were further diluted to the desired concentration in EIA buffer, and then transferred to a 96-well plate coated with a mouse anti-rabbit IgG. Following the addition of the PG tracer (PG-acetylcholinesterase) and anti-PG antibodies, the plate was then incubated overnight at room temperature. The plate was then washed with 10 mM potassium phosphate buffer (pH 7.4) containing 0.01% sodium azide and 0.05% Tween 20 for removal of any unbound reagent. Ellman's reagent (200 μl) was added to each well and the plate was incubated at 37 °C, until the OD_{412} of the control wells reach to 0.5–1.0. The data were presented as the percentage of inhibition relative to heat inactive COX-2 control samples.

2.2.4. Preparation of bone marrow dendritic cells (BMDCs) from mice. Female C57BL/6 (H-2^b) 4–6 week-old mice were purchased from National Laboratory Animal Center (Taipei, Taiwan). They were housed at the facility of Taichung Veterans General Hospital (Taichung, Taiwan). This experiment was carried out in strict accordance with the recommendations in the Guide for the Care and Use of Laboratory Animals of the National Institutes of Health. The protocols were approved by the Institutional Animal Care and Use Committee of Taichung Veterans General Hospital (permit number: La-100824). Mice were euthanized for bone tissue collection by CO_2 asphyxiation and made to minimize pain and suffering. Mice were sacrificed by dislocation of cervical vertebrae. Femurs and tibias were obtained, muscle tissues were removed with gauze, and the bones were placed in a 10 mm dish containing 70% alcohol. After 1 min, the bones were washed twice with phosphate buffered saline (PBS) and transferred into a fresh dish containing RPMI 1640 supplemented with 10% fetal bovine serum, 2 mM glutamine,

and 1% penicillin/streptomycin (10 000 units per ml and 10 μg ml^{-1}, respectively) (Invitrogen, Carlsbad, CA). Both ends were cut off the bones, and then the marrow was flushed out with 5–10 ml of RPMI1640 using a syringe and 25-gauge needle. The tissue was suspended and passed through a nylon mesh to remove small pieces of bone and debris, and red cells were lysed with RBC lysis buffer. The remaining cells were washed with PBS and resuspended in medium, and 7–10 × 10^5 cells per well were placed to 24-well plates in 1 ml of medium supplemented with 10 ng ml^{-1} recombinant mouse granulocyte macrophage colony stimulating factor (rmGM-CSF). Cells were incubated at 37 °C in a 5% CO_2 humidified atmosphere. The cultures were usually fed every 2 days, and non-adherent cells were harvested on day 7. These cells were analyzed by flow cytometry for the expression of CD11c, which is a marker for the differentiation of bone marrow dendritic cells (BMDCs). These BMDCs were harvested and used for experiments.

2.2.5. Measurement of cytokine. The supernatants were collected from bone marrow dendritic cell culture (1 × 10^6/ml) that had been pretreated with the indicated inhibitors for 1 hour and then stimulated with lipopolysaccharide (LPS) (100 ng ml^{-1}, Sigma-Aldrich) for 5 hours. Each experiment, performed in triplicate, included a vehicle control (cells treated with 0.1% DMSO only) and a positive control (cells treated with LPS only). The produced cytokines (IL-1β, TNF-α, IL-6, and IL-12) were measured by using enzyme-linked immunosorbent assays (ELISAs, eBioscience, San Diego, CA) according to the manufacturer's recommendations.

2.2.6. Cytotoxicity assay. Bone marrow dendritic cells (BMDCs) were treated with inhibitors (dissolved in DMSO) in the presence of LPS for 6 hours, and then harvested and stained using a Cell Counting Kit-8 (CCK-8; Sigma). Briefly, 20 μg of CCK8 reagent was added to each well of ELISA plate, and incubated at 37 °C for 24 hours. Subsequently, the supernatants were collected, and OD_{490} was measured by an ELISA reader (TECAN).

2.2.7. Statistical analysis. The results are expressed as means ± SD of at least three experiments. Statistical significance was evaluated by the Student's *t* test. Differences among means were considered significant when $P < 0.05$.

3. Results

3.1. Molecular docking and construction of docking-based pharmacophore model

Molecular docking analyses were performed using the GOLD docking program to generate ligand docking conformations. The GOLD docking program employs a genetic algorithm (GA) to search the complete range of ligand conformations that can bind with the active site of the target protein. To generate the docking poses of the selected inhibitors (Fig. 1 and 2), all molecules were initially processed as follows: (a) two-dimensional (2D) structures were converted into three-dimensional (3D) structures, (b) H atoms were added, and (c) charges were added. To validate the accuracy of our molecular docking setting,

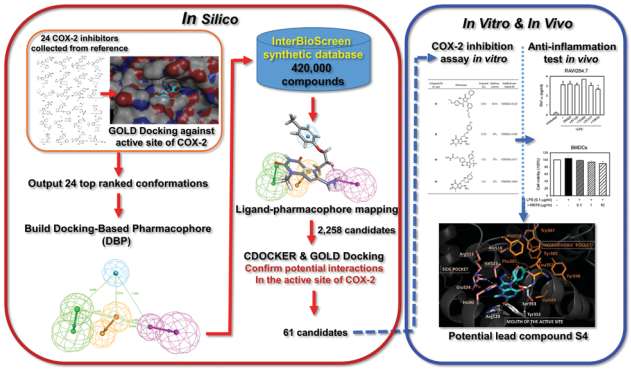

Fig. 1 Flowchart of the combination of structure-based molecular docking and ligand-based pharmacophore modeling to construct the docking-based pharmacophore model, DBP, which consists of crucial complementary functional groups for COX-2 inhibition and was applied to identify potential selective COX-2 inhibitors.

the selective inhibitor SC-558 was redocked into the active site of COX-2 (PDB ID: 1CX2). The resultant RMSD between the crystallized complex structure and the docking pose of SC-558 was approximately 0.5 Å (Fig. 4A). The same docking procedure was used for the 24 selected inhibitors (Fig. 2) to generate docking conformations. Each top ranked docking conformation of the 24 inhibitors was subjected to ligand-based pharmacophore modeling. These 24 docked and structurally diverse COX-2 inhibitors, with IC_{50} spanning 5 orders of magnitude (1.7–70 000 nM) were used as the training set (Fig. 2 and Table 1). DBP hypotheses (Table 2) were developed on the basis of the top ranked docking conformations of the training set inhibitors by using the 3D-quantitative structure–activity relationship pharmacophore generation (HypoGen) module in Discovery Studio 4. All calculations were performed on Advanced Large-scale Parallel Supercluster at the National Center for High-performance Computing, Taiwan. Moreover, four pharmacophore features—hydrogen-bond donor (HBD), hydrogen-bond acceptor (HBA), hydrophobic aromatic (HA), and ring aromatic (RA)—were considered by the HypoGen module during hypothesis generation. The HypoGen module was set to determine pharmacophore models containing zero, one, two, or three features among HBA, HBD, HA, and RA. Finally, the top 10 scoring hypotheses including these four pharmacophore features for each set were exported (Table 2).

The HypoGen module generated 10 hypotheses; the top six hypotheses had the same common features, namely one each of HBD, HBA, HA, and RA (Table 2). The top-ranked pharmacophore model, **Hypo1** (Fig. 5B), demonstrated optimal predictive power and statistical significance, as indicated by a high correlation coefficient (r = 0.92), a low RMSD (1.17), and the highest cost difference (Δcost = 79.02). The HypoGen module uses two essential theoretical cost calculations to determine the success of any pharmacophore hypothesis.[53] Statistically, the fixed cost value of the top 10 hypotheses was 91.35, null cost value was 187.46, configuration cost value was 9.50, and highest cost difference between null and total costs was 79.02. Accordingly, the high correlation coefficient of 0.92 and the lowest

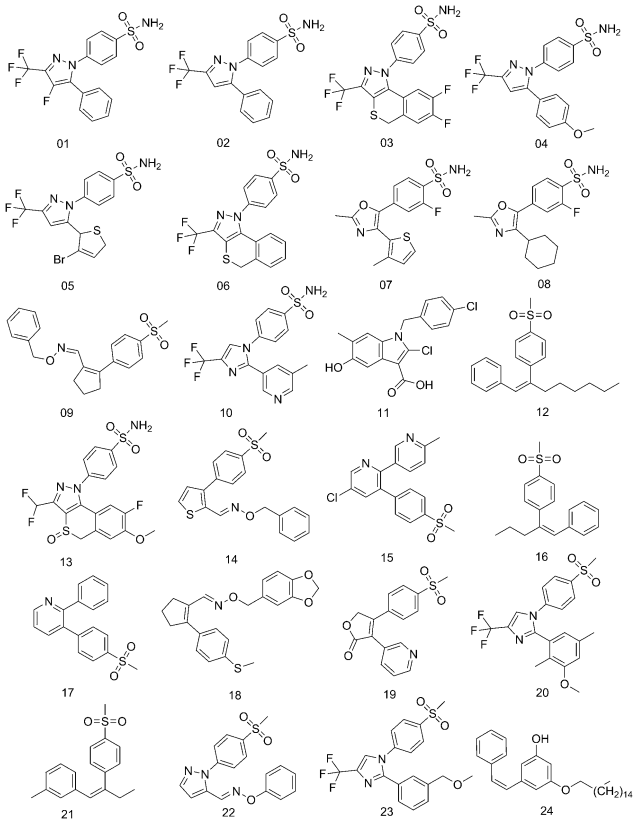

Fig. 2 Chemical structures of all 24 training set molecules used for docking-based pharmacophore generation.

Table 2 Ten pharmacophore hypotheses generated by docking pose Cox-2 inhibitors

Hypo no.	Total cost	Cost difference[a]	Error cost	RMS deviation	Training set (*r*)	Feature[b]
1	108.44	79.02	97.23	1.17	0.92	HBA, HBD, HA, RA
2	109.61	77.85	98.82	1.23	0.91	HBA, HBD, HA, RA
3	111.54	75.92	100.04	1.27	0.91	HBA, HBD, HA, RA
4	111.63	75.83	100.64	1.29	0.90	HBA, HBD, HA, RA
5	115.52	71.94	104.86	1.42	0.88	HBA, HBD, HA, RA
6	115.57	71.89	104.66	1.41	0.88	HBA, HBD, HA, RA
7	117.06	70.40	104.21	1.40	0.88	HBA, HBD
8	117.37	70.09	104.79	1.42	0.88	HBA, HBD
9	119.00	68.46	107.36	1.49	0.87	HBA, HBD, RA
10	119.30	68.16	107.37	1.49	0.87	HBA, HBD, RA

[a] (Null cost – total cost), null cost = 187.46, fixed cost = 91.35, configuration cost = 9.50. All costs are units of bits. [b] HBA, hydrogen-bond acceptor; HBD, hydrogen-bond donor; HA, hydrophobic aromatic; RA, ring aromatic.

RMSD of 1.17 revealed that **Hypo1** had optimal predictive ability and could be used in the subsequent experiments. Furthermore, **Hypo1** accurately predicted the activities of the 24 training set compounds (Table 1). All training set compounds were classified as follows: highly active (≤200 nM, denoted by +++), moderately active (201–2000 nM, denoted by ++), and inactive (>2000 nM, denoted by +). Table 1 presents the actual and estimated activities of the 24 training set compounds. The difference between the estimated and actual activity is represented as an

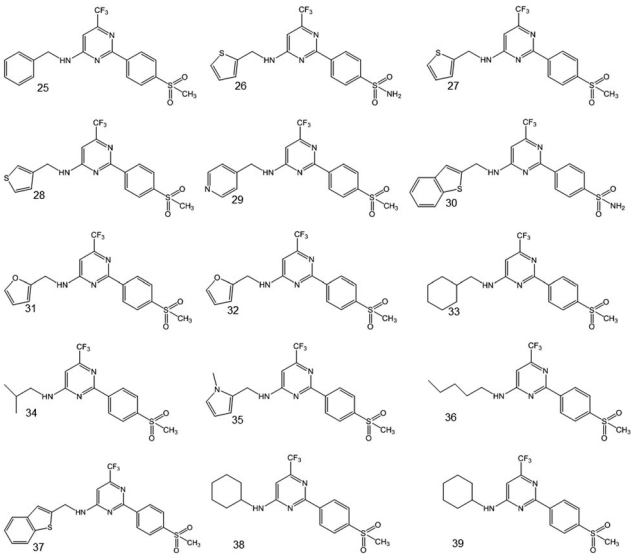

Fig. 3 Chemical structures of all 15 test set molecules used for Hypo1 pharmacophore model validation.

error. A negative sign of the error denotes that the actual activity was higher than the estimated activity. Briefly, all training set compounds were correctly predicted in their activity category except for compounds **9**, **11**, **12** and **14**. The predicting accuracy of successful rates of **Hypo1** to training set (83.3%) and test set (Fig. 3) compounds[10] (86.6%) (Table 3), respectively, revealed favorable predictive ability and is a reliable for further study. **Hypo1** consists of one each of HBD, HBA, HA, and RA (Fig. 5B). The mapping of **Hypo1** with compound **1** of the training set inhibitors is shown in Fig. 5A: all features of **Hypo1** well-fitted with the functional groups of compound **1**, except for HBA. Moreover, the cross-validation was conducted by using the Cat-Scramble module[54] implemented in CATALYST of Discovery Studio 4. This validation procedure is based on Fisher's randomization test.[55] Cross-validation randomizes the activity data among the training set compounds and generates pharmacophore model by means of the same features and parameters as constructing the original **Hypo1** hypotheses. In order to achieve a confidence level of 95% (significance = $[1 - (1 + 0)/(19 + 1)] \times 100\% = 95\%$), 19 random hypotheses were generated (Table 4). The results show that all 19 hypotheses after randomization exhibit poor performance than **Hypo1**. Hence, the cross-validation confirmed the correlation between the structures and experimental activities in the training sets, and reveals the strong confidence on **Hypo1**.

3.2. Ligand pharmacophore mapping for screening novel COX-2 inhibitors

To identify novel COX-2 inhibitors, **Hypo1** was used for ligand pharmacophore mapping to screen approximately 420 000 compounds from the InterBioScreen synthetic database. Compounds matching all the features of **Hypo1** and fitting values over 9 bits were selected as potential candidates. Approximately 2258 of the 420 000 compounds were selected and subjected to CDOCKER and GOLD molecular docking to confirm their

Table 3 Actual and predicted IC_{50} values (nM) of the test set inhibitors based on the **Hypo1**

	Pharmacophore **Hypo1**				
Compound no.	Actual IC_{50} (nM)	Estimated IC_{50} (nM)	Error[b]	Actual scale[a]	Estimated scale[a]
25	71	134.39	1.89	+++	+++
26	157	1.2	−10	+++	+++
27	2	158	79	+++	+++
28	46	138	3	+++	+++
29	298	186.6	−0.62	++	+++
30	140	0.97	−0.0069	+++	+++
31	140	166.7	1.19	+++	+++
32	83	137.2	1.65	+++	+++
33	1480	565	−0.38	++	++
34	789	599	−0.76	++	++
35	28	142	5.07	+++	+++
36	728	561.7	−0.77	++	++
37	293	71.4	0.24	++	+++
38	238	735.7	3.09	++	++
39	475	693.7	1.5	++	++

[a] Activity scale: highly active ($IC_{50} \leq 200$ nM, +++), moderately active (200 nM $< IC_{50} \leq 2000$ nM, ++), and inactive ($IC_{50} > 2000$ nM, +). [b] The difference between estimated and actual activity values is represented as an error (ratio between the estimated and actual activities), and it is assigned a negative symbol if the actual activity is higher than the estimated one. (The 15 COX-2 inhibitors used as test set were retrieved from literature.[53])

Table 4 Results from cross-validation using CatScramble in CATALYST

Results for unscrambled Hypo1					
Total cost = 108.44; Correlation = 0.92					
Results for scrambled					
Trial number	1	2	3	4	5
Total cost	171.025	156.492	171.62	160.151	167.851
Correlation (r)	0.533412	0.662831	0.538378	0.626448	0.556626
Trial number	6	7	8	9	10
Total cost	181.499	151.049	156.477	145.194	153.054
Correlation (r)	0.380341	0.675666	0.693906	0.710476	0.680545
Trial number	11	12	13	14	15
Total cost	146.979	162.627	152.619	158.824	146.979
Correlation (r)	0.706137	0.599066	0.665317	0.599282	0.706137
Trial number	16	17	18	19	
Total cost	167.996	171.761	154.075	169.722	
Correlation (r)	0.629668	0.50495	0.673595	0.534181	

potential interactions with COX-2. In CDOCKER molecular docking, each compound was used to generate 10 random conformations at different heating and cooling temperatures by using CHARMM-based molecular dynamics, and these conformations were docked into the active site of COX-2. The interaction energy was ranked by CDOCKER. In GOLD molecular docking, to find optimized interaction conformations, each compound generated 225 random conformations that were subjected to 500 000 GA operations. Importantly, five well-known COX-2 inhibitors (Fig. 6) were docked into the active site of COX-2. Among them, Lumiracoxib obtained the lowest CDOCKER interaction energy (CIE = 39.62) and GOLD fitness score (GSF = 51.89); these values were used as basic thresholds for compound selection. Approximately 61 potential

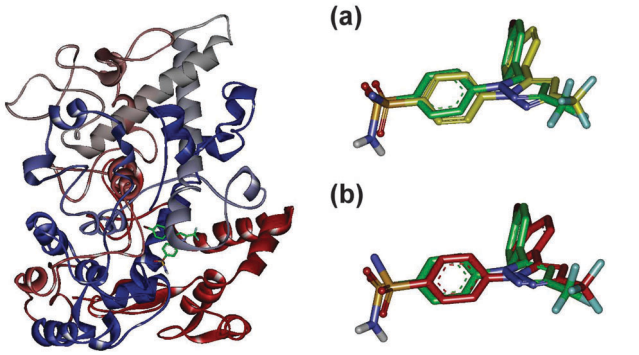

Fig. 4 The inhibitor, SC-558, in complex with the crystal structure of COX-2 (PDB entry code, 1CX2). (A) Superposition of re-docked SC-558 (yellow) by CDOCKER and original crystal SC-558 (green) structure (RMSD: ~0.5 Å). (B) Superposition of re-docked SC-558 (red) by GOLD and original crystal SC-558 (green) structure (RMSD: ~0.5 Å).

candidates (data not shown), whose CIE and GSF were higher than those of Lumiracoxib, were chosen to evaluate their inhibitory activities against human COX-2.

3.3. Inhibitory activities against COX-2

COX-2 inhibition decreases the production of proinflammatory mediators. Thus, we further evaluated COX-2 activity by assessing the generation of the proinflammatory mediator, prostaglandin E2 (PGE2). The inhibitory activity of the selected compounds against human recombinant COX-2 was examined *in vitro*. Human recombinant COX-2 protein was incubated with 87 μM of each compound at 37 °C, and the amount of PGE2 generated was measured through enzyme immunoassay (EIA). Four compounds, **S1**, **S2**, **S3**, and **S4**, exhibited apparent inhibitory activities against COX-2 (39.4%, 48%, 50%, and 55%, respectively) at 87 μM (Table 5).

3.4. Anti-inflammatory effects of S4

The lipopolysaccharide (LPS)-stimulated cell culture model was employed to study the anti-inflammatory effects of **S1**, **S2**, **S3**, and **S4** *in vitro*. Mouse macrophage RAW264.7 cells were pre-treated with the test compounds for 1 h and stimulated with LPS for another 5 h, and the levels of generated tumor necrosis factor (TNF)-α were assessed through ELISA. Compared with the control and **S1**-, **S2**-, and **S3**-treated cells, **S4**-treated cells showed an obvious suppression of LPS-induced TNF-α production (Fig. 7A), thus revealing the potential anti-inflammatory activity of **S4**. To verify this anti-inflammation activity, the production of primary inflammatory cytokines (IL-1β, TNF-α, IL-6, and IL-12, which signal dendritic cell activation) in LPS-treated bone marrow dendritic cells (BMDCs) with and without **S4** pretreatment was assessed through ELISA. The production of IL-1β, TNF-α, IL-6, and IL-12 was considerably reduced after pretreating with 10 μg ml^{-1} of **S4** (Fig. 7B), indicating that **S4** has a great potential to inhibit inflammation in BMDCs. To clarify whether the suppressive effect of **S4** resulted from the compound's cytotoxicity, BMDCs were cotreated with LPS and **S4** for 5 h, following which cell viability was estimated. **S4** did not cause considerable BMDC death at

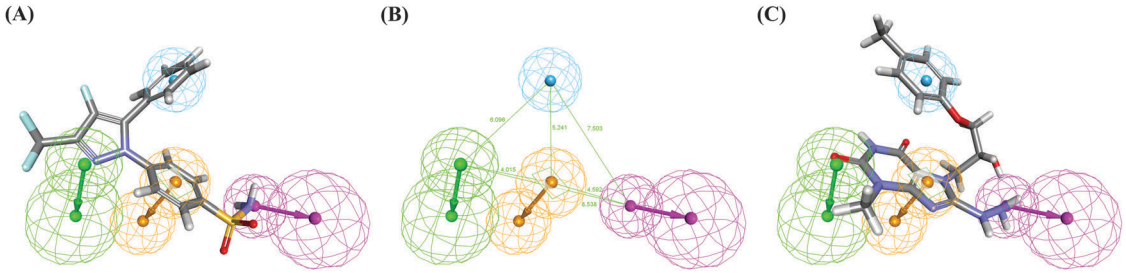

Fig. 5 Schematic representation and structural information of pharmacophore model, **Hypo1**, compound **1** and **S4** molecules. (A) Compound **1** (ball and stick) fits with pharmacophore model, **Hypo1**. (B) Features at a specific distance correspond to the pharmacophore model, **Hypo1**. (Features are color-coded as follows: blue, hydrophobic; green, hydrogen-bond acceptor; magenta, and hydrogen-bond donor) (C) mapping of compound, **S4**, (ball and stick) onto the pharmacophore model, **Hypo1**.

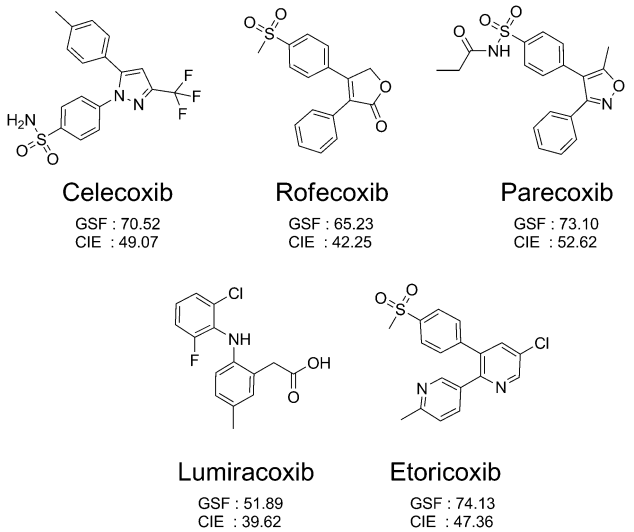

Fig. 6 The chemical structures, GOLD Score Fitness (GSF) and CDOCKER Interaction Energy (CIE) of five known COX-2 inhibitors.

10 μg ml^{-1} (Fig. 7C). These findings revealed that **S4** exhibited inhibitory activity against COX-2 *in vitro* as well as showed strong anti-inflammatory activity without causing major cytotoxicity *in vivo*.

Table 5 The inhibitory efficiency of candidate compounds

Compound ID (87 μM)	2D structure	Inhibitory activity (%)	InterBioScreen catalog ID
S1	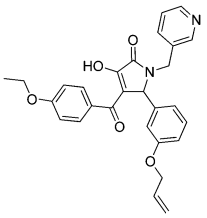	39.4	STOCK3S-81120
S2	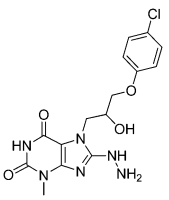	48	STOCK1S-15490
S3	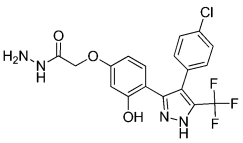	50	STOCK4S-51317
S4	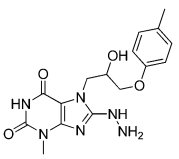	55	STOCK5S-10619

4. Discussion

Previously, Chopra *et al.*[9] establish a pharmacophore model from 24 known COX-2 inhibitors by using common ligand-based pharmacophore generation strategy, however no further applications were carried out. Therefore, in this study we combined structure- and ligand-based pharmacophore generation and employed the same 24 COX-2 inhibitors to construct a more precise pharmacophore model and use it to identify novel COX-2 inhibitors (Fig. 1). By employing the top ranked docking conformations of 24 known COX-2 inhibitors, we specifically build a rational and reliable **DBP** model, **Hypo1**, containing major complementary functional groups for COX-2 inhibition. Subsequently, the use of ligand pharmacophore mapping (**Hypo1**) reduced the number of compounds from 420 000 (from InterBioScreen synthetic database) to 2258. CDOCKER and GOLD molecular docking was performed to study the interaction of these 2258 compounds with COX-2. Finally, 61 potential candidates were identified. COX-2 inhibition assay demonstrated that compound **S4** exhibited exceptional COX-2 inhibitory ability and that the ligand pharmacophore mapping result showed that all functional groups of **S4** fitted well with the features of **Hypo1** (Fig. 5C). These results indicated that the **DBP** model, **Hypo1**, consisting of essential complementary functional features, is highly reliable and capable of precisely screening potent COX-2 inhibitors. To design novel and selective COX inhibitors, understanding the differences between COX-1 and COX-2 is essential. COX-1 (PDB ID: 1PRH) and COX-2 (PDB ID: 1CX2) show nearly identical tertiary structures (α-carbons RMSD: 0.9 Å), and share 61% sequence identity, which increases to 87% when only active

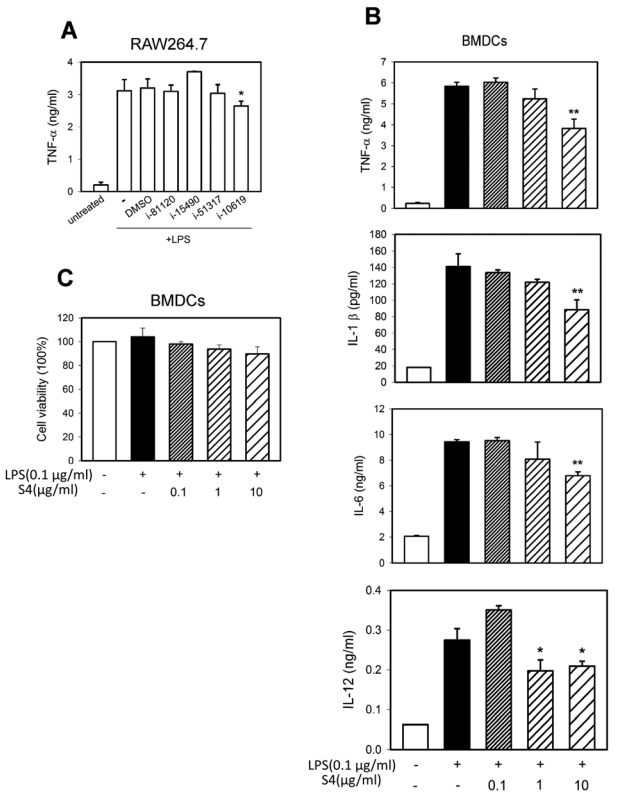

Fig. 7 The anti-inflammation effects of compounds **S1**, **S2**, **S3**, and **S4**. (A) Compound, **S4**, shows the most significant anti-inflammation ability among all other compounds. (Mouse macrophage RAW264.7 cells were pre-treated with the test compounds 1 h and stimulated with LPS for 5 h, and TNF-α production was determined by ELISA.) (B) The considerable down regulations of primary inflammatory cytokines (IL-1β, TNF-α, IL-6, and IL-12) were observed under the treatment of **S4** (10 μg ml^{-1}). Mouse BMDCs were pre-treated with different doses of **S4** for 1 h and then co-treated with 0.1 μg ml^{-1} LPS for 5 h. Supernatants were collected and the levels of cytokines were determined by ELISA. (C) Compound, **S4** (10 μg ml^{-1}), shows no significant cytotoxicity to BMDCs. The cytotoxicity of **S4** on BMDCs was analyzed by Cell Counting Kit-8 (CCK-8).

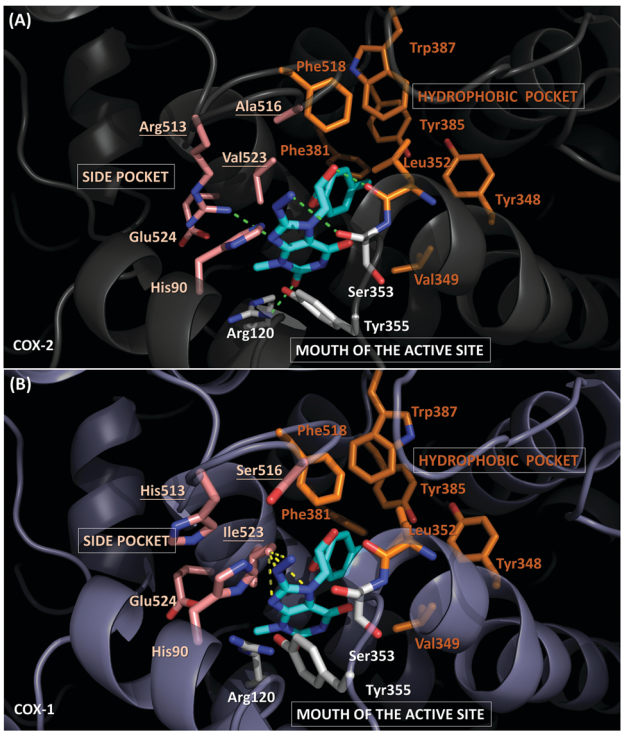

Fig. 8 Illustrations of structural interactions of compound, **S4** with COX-1 and COX-2. (A) The molecular docking model of compound, **S4** (sticks, colored in cyan), in the active site of COX-2. (B) The docking model of **S4** in complex with active site of COX-1. (Residues in the hydrophobic pocket, mouth of the active site, and side pocket are shown as sticks and colored in orange, white, and pink, respectively. The hydrogen bonds are presented as green dash lines, and the steric clashes are denoted in yellow dash lines.)

site residues were compared (data not shown). The active site of COX has three regions: a hydrophobic pocket beneath the heme group, the mouth of the active site, and a side pocket (Fig. 8). The residues in the hydrophobic pocket and the mouth of the active site are highly conserved, but those in the side pocket show variety in COX-1 (Arg513, Ala516, and Val523) and COX-2 (His513, Ser516, and Ile523) (Fig. 8). Selective inhibitors can be designed to interact with the nonconserved residues between COX-1 and COX-2. Tricyclic inhibitors, which are larger than traditional NSAIDs, interact with the nonconserved residue Arg513 of COX-2 but not with His513 of COX-1.[56] Val523 in COX-2, located on the side pocket of the COX binding site, is another observed nonconserved residue (Ile523 in COX-1). Arg513 and Val523 are essential for COX-2-selective inhibitor binding.[57] Arg513 facilitates polar interaction with a selective COX-2 inhibitor, such as rofecoxib,[56] whereas Ile523, because of considerable steric hindrance, renders difficult the binding of inhibitors to the lateral pocket of COX-1.[58] In addition, Val523 acts as a modulator of the kinetic/dynamic behavior of inhibitors; that is, the replacement of Val523 to Ile523 in COX-2 changes the behavior of tricyclic inhibitors from time-dependent to time-independent.[57,59] All these varieties and features are critical for developing selective COX-2 inhibitors. Molecular docking analyses revealed that **S4** well-fitted in the active site of COX-2 (Fig. 8A). The benzene moiety of **S4** occupies itself in the hydrophobic pocket and interacts with the surrounding hydrophobic residues (Tyr348, Val349, Leu352, Phe381, Tyr385, Trp387, and Phe518). In addition, hydrogen bond interactions were observed among **S4** and residues in the hydrophobic pocket (Leu352), in the mouth of the active site (Ser353 and Arg120), and in the side pocket (Arg513). However, the molecular docking model of **S4** in the active site of COX-1 (Fig. 8B) demonstrated that His513 of COX-1 corresponded with Arg513 of COX-2 and showed no hydrogen bonding with **S4**. Moreover, Ile523 in the side pocket of COX-1 exhibited considerable steric clash with **S4**, implying that the large Ile523 produced steric hindrance, which hindered the binding of **S4** to the lateral pocket of COX-1. These results indicated that **S4** has a strong potential to selectively inhibit COX-2.

NSAIDs, such as aspirin, ibuprofen, indomethacin, and naproxen, are most widely used in treating inflammation and pain.[60–70] However, they exhibit harmful side effects, such as ulcers, perforation, GI tract bleeding, and nephrotoxicity.[15–17]

Table 6 The candidate ADMET prediction[a]

ddH_2O		ADMET prediction				
Compounds	Inhibitory activity (%)	BBB	Absorption	CYP2D6	Hepatotoxicity	PPB
S1	39.4	2	0	False	False	False
S2	48	4	1	False	False	False
S3	50	4	1	False	False	False
S4	55	4	1	False	False	False

[a] The ADMET prediction was performed by using ADMET descriptor discovery implemented by the Discovery Studio 4 (Accelrys Inc., San Diego, CA, USA). IC50: 50% inhibitory concentration. BBB: it predicts the level of blood–brain penetration (blood brain barrier, BBB) after oral administration (0, very high; 1, high; 2, medium; 3, low; 4, undefined; 5, warning: molecules with one or more unknown AlogP98 types). Absorption: it predicts the human intestinal absorption level of each compound (0, good; 1, moderate; 2, low; 3, very low). CYP2D6 prediction: it predicts cytochrome P450 2D6 enzyme inhibition. Hepatotoxicity: it predicts the occurrence of dose-dependent human hepatotoxicity. PPB (Plasma Protein Binding Prediction): it predicts likelihood that a compound will be highly bound to carrier proteins in the blood.

Both the anti-inflammatory effects and side effects are strongly associated with COX isoforms. The COX-1 inhibitory activities of nonselective COX inhibitors or COX-1 selective inhibitors causing GI tract side effects are major problems with the use of traditional NSAIDs.[15–17,71] Moreover, the inhibitory activities of other traditional NSAIDs against COX-1 cause respiratory and cutaneous hypersensitivities and cross-reactivity.[72] Selective COX-2 inhibitors are crucial for treating COX-2 action-derived diseases (*e.g.*, OA, RA, and pyrexia) and various inflammatory diseases and syndromes[73] with no clinical concerns related to COX-1 inhibition. Consequently, several selective COX-2 inhibitors, namely etoricoxib, nimesulide, celecoxib, valdecoxib, and rofexocib, have been developed and used to treat OA and RA without GI damage.[37–40] The selective COX-2 inhibitor, rofecoxib, was recently withdrawn from the market because of its adverse cardiovascular side effects.[42] This has raised the concern regarding the safety of selective COX-2 inhibitors. Thus, new selective COX-2 inhibitors with a high safety profile must be discovered. In this study, we identified a novel and potential selective COX-2 inhibitor, **S4**, showing exceptional COX-2 inhibitory activity compared with all other COX-2 inhibitors, thereby revealing its potential anti-inflammatory activity (Table 3). This was confirmed by the results of the estimation of inflammatory cytokine production by BMDCs; IL-1β, TNF-α, IL-6, and IL-12 production was considerably reduced after pretreating with 10 μg ml^{-1} **S4**, but it did not cause considerable BMDC death (Fig. 7B and C). Thus, **S4** considerably inhibited human COX-2 activity *in vitro* and suppressed LPS-induced inflammatory cytokine production in BMDCs *in vivo* without considerable cytotoxicity (Fig. 7C). The pharmacokinetic profile of the top hits (**S1–S4**) under investigation was predicted by means of five precalculated ADMET (Absorption, Distribution, Metabolism, Excretion, and Toxicity) models provided by the Discovery Studio 4 (Table 6). The results show that the top hits (**S1–S4**) are within the high-to-low oral intestinal absorption level, low-to-undefined level of blood–brain penetration, and without hepatotoxicity. In addition, **S1–S4** are predicted to be false in cytochrome P450 2D6 enzyme inhibition and binding with carrier proteins in the blood. Collectively, these findings together with the ADMET analysis, the drug design strategy, and the molecular docking analysis showed that **S4** has a strong potential as a selective COX-2 inhibitor and could be further used in anti-inflammatory treatment. Notably, the potential cardiovascular risks associated with highly selective COX-2 inhibition (relative to COX-1) indicates that further modification of the identified compound, **S4**, is needed to allow for some COX-1 inhibition rather than to be too highly selective for COX-2. In addition, a growing body of evidence shows that COX-2 contributes to carcinogenesis, and studies of selective COX-2 inhibitors in the treatment of cancers and neurodegenerative disorders reveal the potential therapeutic development and application of **S4**.

5. Conclusion

We combined structure-based drug design (molecular docking) and ligand-based drug design (pharmacophore modeling) to build a reliable **DBP** model, **Hypo1**, for screening selective COX-2 inhibitors. Four compounds, **S1**, **S2**, **S3**, and **S4**, identified by pharmacophore mapping, apparently inhibited COX-2 activity at 87 μM. **S4** exhibited inhibitory activity against COX-2 *in vitro* as well as showed potential anti-inflammatory activity *in vivo* without causing major cytotoxicity. Molecular docking analyses showed that **S4** fitted well in the active site of COX-2 but exhibited considerable steric clash with that of COX-1, revealing the selective inhibition ability of **S4** against COX-2. Unprecedentedly, we demonstrated a successful strategy of employing molecular docking and ligand-based pharmacophore modeling to rationally construct a novel **DBP** model, consisting of complementary functional features necessary for selective COX-2 inhibition. **S4** has a strong potential for development as an anti-inflammatory and even an anticancer agent.

Conflicts of interest

The authors declare no competing financial interests.

Abbreviations

2D	Two-dimensional
3D	Three-dimensional
BMDCs	Bone marrow dendritic cells
CADD	Computer-aided drug design
CIE	CDCOCKER interaction energy

COX	Cyclooxygenase
DBP	Docking-based pharmacophore
EIA	Enzymeimmunoassay
ELISA	Enzyme-linked immunosorbent assay
GA	Genetic algorithm
GOLD	Genetic optimization for ligand docking
GSF	GOLD fitness score
GI	Gastrointestinal
LBDD	Ligand-based drug design
LPS	Lipopolysaccharide
IL	Interleukin
NSAIDs	Non-steroidal anti-inflammatory drugs
OA	Osteoarthritis
PGs	Prostaglandins
PGE2	Prostaglandin E2
RA	Rheumatoid arthritis
SBDD	Structure-based drug design
TNF	Tumor necrosis factor

Acknowledgements

We thank Dr Kuei-Chung Shih and Dr Chuan-Yi Tang for fruitful discussion and help. We are grateful to the National Center for High-performance Computing for computer time and facilities. The computational work using GOLD and Discovery Studio were conducted at the National Center for High-performance Computing, Taiwan. This work was supported by Ministry of Science and Technology [MOST 103-2320-B-077-001-MY3 to K.-C. T.], Taipei, Taiwan.

References

1 A. Diaz, K. P. Chepenik, J. H. Korn, A. M. Reginato and S. A. Jimenez, *Exp. Cell Res.*, 1998, **241**, 222–229.
2 M. E. Turini and R. N. DuBois, *Annu. Rev. Med.*, 2002, **53**, 35–57.
3 D. Wang and R. N. Dubois, *Semin. Oncol.*, 2004, **31**, 64–73.
4 K. Seibert, Y. Zhang, K. Leahy, S. Hauser, J. Masferrer, W. Perkins, L. Lee and P. Isakson, *Proc. Natl. Acad. Sci. U. S. A.*, 1994, **91**, 12013–12017.
5 G. P. O'Neill and A. W. Ford-Hutchinson, *FEBS Lett.*, 1993, **330**, 156–160.
6 S. Kargman, S. Charleson, M. Cartwright, J. Frank, D. Riendeau, J. Mancini, J. Evans and G. O'Neill, *Gastroenterology*, 1996, **111**, 445–454.
7 M. J. Thun, S. J. Henley and C. Patrono, *J. Natl. Cancer Inst.*, 2002, **94**, 252–266.
8 G. P. Boland, I. S. Butt, R. Prasad, W. F. Knox and N. J. Bundred, *Br. J. Cancer*, 2004, **90**, 423–429.
9 M. Chopra, R. Gupta, S. Gupta and D. Saluja, *J. Mol. Model.*, 2008, **14**, 1087–1099.
10 U. A. Shah, H. S. Deokar, S. S. Kadam and V. M. Kulkarni, *Mol. Diversity*, 2010, **14**, 559–568.
11 S. Shankar, S. Ganapathy, S. R. Hingorani and R. K. Srivastava, *Front. Biosci.*, 2008, **13**, 440–452.
12 S. Shankar, Q. Chen and R. K. Srivastava, *J. Mol. Signaling*, 2008, **3**, 7.
13 M. Barone, G. Pannuzzo, A. Santagati, A. Catalfo, G. De Guidi and V. Cardile, *Molecules*, 2014, **19**, 6106–6122.
14 J. H. Herman and E. V. Hess, *Am. J. Med.*, 1984, **77**, 16–25.
15 L. Laine, *J. Cardiovasc. Pharmacol.*, 2006, **47**(suppl 1), S60–66.
16 Z. A. Radi and N. K. Khan, *Exp. Toxicol. Pathol.*, 2006, **58**, 163–173.
17 T. D. Warner, F. Giuliano, I. Vojnovic, A. Bukasa, J. A. Mitchell and J. R. Vane, *Proc. Natl. Acad. Sci. U. S. A.*, 1999, **96**, 7563–7568.
18 E. Manivannan, S. Prasanna and S. C. Chaturvedi, *Indian J. Biochem. Biophys.*, 2004, **41**, 179–183.
19 J. J. Li, G. D. Anderson, E. G. Burton, J. N. Cogburn, J. T. Collins, D. J. Garland, S. A. Gregory, H. C. Huang, P. C. Isakson and C. M. Koboldt, *et al.*, *J. Med. Chem.*, 1995, **38**, 4570–4578.
20 J. C. Boehm, J. M. Smietana, M. E. Sorenson, R. S. Garigipati, T. F. Gallagher, P. L. Sheldrake, J. Bradbeer, A. M. Badger, J. T. Laydon, J. C. Lee, L. M. Hillegass, D. E. Griswold, J. J. Breton, M. C. Chabot-Fletcher and J. L. Adams, *J. Med. Chem.*, 1996, **39**, 3929–3937.
21 I. K. Khanna, R. M. Weier, Y. Yu, P. W. Collins, J. M. Miyashiro, C. M. Koboldt, A. W. Veenhuizen, J. L. Currie, K. Seibert and P. C. Isakson, *J. Med. Chem.*, 1997, **40**, 1619–1633.
22 C. J. Hawkey, *Lancet*, 1999, **353**, 307–314.
23 M. Tsujii, S. Kawano, S. Tsuji, H. Sawaoka, M. Hori and R. N. DuBois, *Cell*, 1998, **93**, 705–716.
24 A. Bhardwaj, J. Kaur, S. K. Sharma, Z. Huang, F. Wuest and E. E. Knaus, *Bioorg. Med. Chem. Lett.*, 2013, **23**, 163–168.
25 A. S. Kalgutkar and Z. Zhao, *Curr. Drug Targets*, 2001, **2**, 79–106.
26 G. M. Pasinetti, *J. Neurosci. Res.*, 1998, **54**, 1–6.
27 F. Andersohn, S. Suissa and E. Garbe, *Circulation*, 2006, **113**, 1950–1957.
28 T. R. Hegi, T. Bombeli, B. Seifert, P. C. Baumann, U. Haller, M. P. Zalunardo, T. Pasch and D. R. Spahn, *Br. J. Anaesth.*, 2004, **92**, 523–531.
29 G. Rimon, R. S. Sidhu, D. A. Lauver, J. Y. Lee, N. P. Sharma, C. Yuan, R. A. Frieler, R. C. Trievel, B. R. Lucchesi and W. L. Smith, *Proc. Natl. Acad. Sci. U. S. A.*, 2010, **107**, 28–33.
30 C. N. Serhan and B. Levy, *Proc. Natl. Acad. Sci. U. S. A.*, 2003, **100**, 8609–8611.
31 C. J. Smith, Y. Zhang, C. M. Koboldt, J. Muhammad, B. S. Zweifel, A. Shaffer, J. J. Talley, J. L. Masferrer, K. Seibert and P. C. Isakson, *Proc. Natl. Acad. Sci. U. S. A.*, 1998, **95**, 13313–13318.
32 J. L. Masferrer, B. S. Zweifel, P. T. Manning, S. D. Hauser, K. M. Leahy, W. G. Smith, P. C. Isakson and K. Seibert, *Proc. Natl. Acad. Sci. U. S. A.*, 1994, **91**, 3228–3232.
33 L. Gossec, D. van der Heijde, A. Melian, D. A. Krupa, M. K. James, P. F. Cavanaugh, A. S. Reicin and M. Dougados, *Ann. Rheum. Dis.*, 2005, **64**, 1563–1567.
34 B. Hinz, B. Renner and K. Brune, *Nat. Clin. Pract. Rheumatol.*, 2007, **3**, 552–560, quiz 551 p following 589.

35 K. Gottesdiener, T. Schnitzer, C. Fisher, B. Bockow, J. Markenson, A. Ko, L. DeTora, S. Curtis, L. Geissler and B. J. Gertz, *Rheumatology*, 2002, **41**, 1052–1061.
36 J. F. Knudsen, U. Carlsson, P. Hammarstrom, G. H. Sokol and L. R. Cantilena, *Inflammation*, 2004, **28**, 285–290.
37 J. J. Talley, D. L. Brown, J. S. Carter, M. J. Graneto, C. M. Koboldt, J. L. Masferrer, W. E. Perkins, R. S. Rogers, A. F. Shaffer, Y. Y. Zhang, B. S. Zweifel and K. Seibert, *J. Med. Chem.*, 2000, **43**, 775–777.
38 P. Prasit, Z. Wang, C. Brideau, C. C. Chan, S. Charleson, W. Cromlish, D. Ethier, J. F. Evans, A. W. Ford-Hutchinson, J. Y. Gauthier, R. Gordon, J. Guay, M. Gresser, S. Kargman, B. Kennedy, Y. Leblanc, S. Leger, J. Mancini, G. P. O'Neill, M. Ouellet, M. D. Percival, H. Perrier, D. Riendeau, I. Rodger and R. Zamboni, *et al.*, *Bioorg. Med. Chem. Lett.*, 1999, **9**, 1773–1778.
39 T. D. Penning, J. J. Talley, S. R. Bertenshaw, J. S. Carter, P. W. Collins, S. Docter, M. J. Graneto, L. F. Lee, J. W. Malecha, J. M. Miyashiro, R. S. Rogers, D. J. Rogier, S. S. Yu, G. D. Anderson, E. G. Burton, J. N. Cogburn, S. A. Gregory, C. M. Koboldt, W. E. Perkins, K. Seibert, A. W. Veenhuizen, Y. Y. Zhang and P. C. Isakson, *J. Med. Chem.*, 1997, **40**, 1347–1365.
40 I. A. Tavares, P. M. Bishai and A. Bennett, *Arzneim. Forsch.*, 1995, **45**, 1093–1095.
41 N. Bhala, J. Emberson, A. Merhi, S. Abramson, N. Arber, J. A. Baron, C. Bombardier, C. Cannon, M. E. Farkouh, G. A. FitzGerald, P. Goss, H. Halls, E. Hawk, C. Hawkey, C. Hennekens, M. Hochberg, L. E. Holland, P. M. Kearney, L. Laine, A. Lanas, P. Lance, A. Laupacis, J. Oates, C. Patrono, T. J. Schnitzer, S. Solomon, P. Tugwell, K. Wilson, J. Wittes and C. Baigent, *Lancet*, 2013, **382**, 769–779.
42 J. M. Dogne, C. T. Supuran and D. Pratico, *J. Med. Chem.*, 2005, **48**, 2251–2257.
43 A. Zarghi and S. Arfaei, *Iran. J. Pharm. Res.*, 2011, **10**, 655–683.
44 C. Luong, A. Miller, J. Barnett, J. Chow, C. Ramesha and M. F. Browner, *Nat. Struct. Biol.*, 1996, **3**, 927–933.
45 R. G. Kurumbail, A. M. Stevens, J. K. Gierse, J. J. McDonald, R. A. Stegeman, J. Y. Pak, D. Gildehaus, J. M. Miyashiro, T. D. Penning, K. Seibert, P. C. Isakson and W. C. Stallings, *Nature*, 1996, **384**, 644–648.
46 A. L. Blobaum and L. J. Marnett, *J. Med. Chem.*, 2007, **50**, 1425–1441.
47 S. Thangapandian, S. John, S. Sakkiah and K. W. Lee, *J. Mol. Graphics Modell.*, 2010, **29**, 382–395.
48 S. Thangapandian, S. John, S. Sakkiah and K. W. Lee, *Eur. J. Med. Chem.*, 2010, **45**, 4409–4417.
49 M. Liu, L. He, X. Hu, P. Liu and H. B. Luo, *Bioorg. Med. Chem. Lett.*, 2010, **20**, 7004–7010.
50 G. Wu, D. H. Robertson, C. L. Brooks, 3rd and M. Vieth, *J. Comput. Chem.*, 2003, **24**, 1549–1562.
51 Y. Dai, Q. Wang, X. Zhang, S. Jia, H. Zheng, D. Feng and P. Yu, *Eur. J. Med. Chem.*, 2010, **45**, 5612–5620.
52 K. C. Shih, C. W. Shiau, T. S. Chen, C. H. Ko, C. L. Lin, C. Y. Lin, C. S. Hwang, C. Y. Tang, W. R. Chen and J. W. Huang, *Bioorg. Med. Chem. Lett.*, 2011, **21**, 4490–4497.
53 M. Pal and S. Paliwal, *Org. Med. Chem. Lett.*, 2012, **2**, 7.
54 R. Sarma, S. Sinha, M. Ravikumar, M. Kishore Kumar and S. K. Mahmood, *Eur. J. Med. Chem.*, 2008, **43**, 2870–2876.
55 M. L. Teodoro and L. E. Kavraki, *Curr. Pharm. Des.*, 2003, **9**, 1635–1648.
56 O. Llorens, J. J. Perez, A. Palomer and D. Mauleon, *J. Mol. Graphics Modell.*, 2002, **20**, 359–371.
57 E. Wong, C. Bayly, H. L. Waterman, D. Riendeau and J. A. Mancini, *J. Biol. Chem.*, 1997, **272**, 9280–9286.
58 M. L. Price and W. L. Jorgensen, *Bioorg. Med. Chem. Lett.*, 2001, **11**, 1541–1544.
59 Q. Guo, L. H. Wang, K. H. Ruan and R. J. Kulmacz, *J. Biol. Chem.*, 1996, **271**, 19134–19139.
60 C. D. Funk, *Science*, 2001, **294**, 1871–1875.
61 D. L. Simmons, R. M. Botting and T. Hla, *Pharmacol. Rev.*, 2004, **56**, 387–437.
62 H. U. Zeilhofer, *Biochem. Pharmacol.*, 2007, **73**, 165–174.
63 H. R. Kim, E. Y. Kim, J. Cerny and K. D. Moudgil, *J. Immunol.*, 2006, **177**, 6634–6641.
64 R. Y. Kang, J. Freire-Moar, E. Sigal and C. Q. Chu, *Br. J. Rheumatol.*, 1996, **35**, 711–718.
65 C. M. Blatteis, *Pharmacol. Ther.*, 2006, **111**, 194–223.
66 A. A. Romanovsky, M. C. Almeida, D. M. Aronoff, A. I. Ivanov, J. P. Konsman, A. A. Steiner and V. F. Turek, *Front. Biosci.*, 2005, **10**, 2193–2216.
67 A. A. Steiner, A. I. Ivanov, J. Serrats, H. Hosokawa, A. N. Phayre, J. R. Robbins, J. L. Roberts, S. Kobayashi, K. Matsumura, P. E. Sawchenko and A. A. Romanovsky, *PLoS Biol.*, 2006, **4**, e284.
68 S. Li, Y. Wang, K. Matsumura, L. R. Ballou, S. G. Morham and C. M. Blatteis, *Brain Res.*, 1999, **825**, 86–94.
69 J. R. Vane and R. M. Botting, *Thromb. Res.*, 2003, **110**, 255–258.
70 M. Burian and G. Geisslinger, *Pharmacol. Ther.*, 2005, **107**, 139–154.
71 J. A. Mitchell and T. D. Warner, *Br. J. Pharmacol.*, 1999, **128**, 1121–1132.
72 X. Li, L. P. Tao and C. H. Wang, *World J. Gastroenterol.*, 2014, **20**, 12322–12329.
73 S. Hayashi, N. Ueno, A. Murase, Y. Nakagawa and J. Takada, *Eur. J. Med. Chem.*, 2012, **50**, 179–195.